2nd Advanced Optical Metrology Compendium

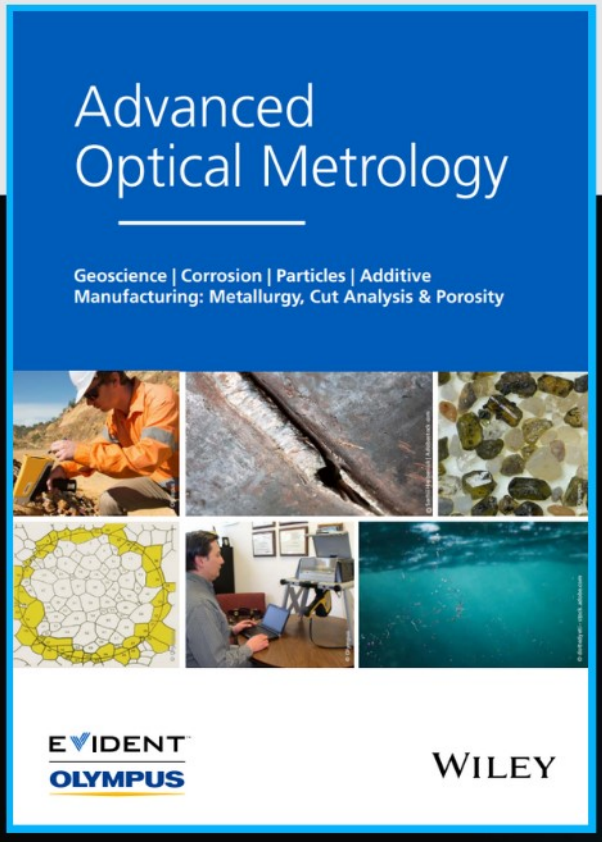

The latest eBook from Advanced Optical Metrology. Download for free.

This compendium includes a collection of optical metrology papers, a repository of teaching materials, and instructions on how to publish scientific achievements.

With the aim of improving communication between fundamental research and industrial applications in the field of optical metrology we have collected and organized existing information and made it more accessible and useful for researchers and practitioners.

EVIDENT
OLYMPUS

WILEY

ADVANCED FUNCTIONAL MATERIALS
www.afm-journal.de

Multifunctional and Wearable Patches Based on Flexible Piezoelectric Acoustics for Integrated Sensing, Localization, and Underwater Communication

Qian Zhang, Yong Wang, Dongsheng Li, Jin Xie, Kai Tao, PingAn Hu, Jian Zhou, Honglong Chang, and Yongqing Fu**

Flexible and wearable sensors are highly desired for health monitoring, agriculture, sport, and indoor positioning systems applications. However, the currently developed wireless wearable sensors, which are communicated through radio signals, can only provide limited positioning accuracy and are often ineffective in underwater conditions. In this paper, a wireless platform based on flexible piezoelectric acoustics is developed with multiple functions of sensing, communication, and positioning. Under a high frequency (≈13 MHz) stimulation, Lamb waves are generated for respiratory monitoring. Whereas under low-frequency stimulation (≈20 kHz), this device is agitated as a vibrating membrane, which can be implemented for communication and positioning applications. Indoor communication is demonstrated within 2.8 m at 200 bps or 4.2 m at 25 bps. In combination with the sensing function, real-time respiratory monitoring and wireless communication are achieved simultaneously. The distance measurement is achieved based on the phase differences of transmitted and received acoustic signals within a range of 100 cm, with a maximum error of 3 cm. This study offers new insights into the communication and positioning applications using flexible acoustic wave devices, which are promising for wireless and wearable sensor networks.

1. Introduction

Flexible and wireless sensors have attracted profound interest owing to their widespread applications in healthcare,[1–3] wearable electronics,[4–7] robotics,[8] and internet of things (IoTs).[9] However, the recently reported flexible sensors based on either capacitance or resistance mechanisms often need an additional antenna to achieve wireless or real-time functions,[10,11] thus increasing the complications and size of the sensing system. Furthermore, communication approaches based on radio frequency (RF) signals often show deteriorated performance, in situations such as in underwater conditions or inside a metal shell,[12,13] thus preventing them from being adopted in underwater vehicles, marine environment monitoring systems, wearable devices for swimming and diving, and/or being embedded into instruments with numerous metal components. On the other hand, the distance measurement based on RF signals, which has been widely studied for the requirement of the positioning of wireless sensor networks (WSNs), could only provide a limited accuracy (e.g., with errors larger than 10 cm).[14–16]

There are huge interest recently in the development of flexible acoustic wave devices, mainly because of their promising properties (such as mechanical bendability, lightweight, cost-effectiveness, biocompatibility, and disposability).[17–20]

Q. Zhang, D. Li, J. Xie, Y. Fu
The State Key Laboratory of Fluid Power and Mechatronic Systems
Zhejiang University
Hangzhou 310027, P. R. China
E-mail: xiejin@zju.edu.cn

Q. Zhang, Y. Wang, Y. Fu
Faculty of Engineering and Environment
University of Northumbria
Newcastle upon Tyne NE1 8ST, UK
E-mail: richard.fu@northumbria.ac.uk

The ORCID identification number(s) for the author(s) of this article can be found under https://doi.org/10.1002/adfm.202209667.

DOI: 10.1002/adfm.202209667

Y. Wang
Key Laboratory of 3D Micro/Nano Fabrication and Characterization of Zhejiang Province, School of Engineering
Westlake University
Hangzhou 310024, P. R. China

K. Tao, H. Chang
Ministry of Education Key Laboratory of Micro and Nano Systems for Aerospace
Northwestern Polytechnical University
Xi'an 710072, P. R. China

P. Hu
MOE Key Lab of Micro-System and Micro-Structures Manufacturing
Harbin Institute of Technology
Harbin 150080, P. R. China

J. Zhou
College of Mechanical and Vehicle Engineering
Hunan University
Changsha 410082, P.R. China

Extensive studies have been done for flexible acoustic wave devices used in various fields such as sensing (temperature,[21] humidity,[22] UV,[23] biosensing,[20,24] strain,[25–28] and pH),[29] acoustofluidics,[30] and flexible RF filter/oscillator.[17] Depending on the structural designs, piezoelectric devices with different vibration modes have been fabricated, e.g., surface acoustic wave (SAW) devices,[31] Lamb wave devices,[32] and film bulk acoustic resonators (FBAR).[33] However, most of these studies are focused more on achieving their inherent flexibility. It should be addressed that in order to achieve good flexibility of such devices, thickness and stiffness of the film and substrates are generally relatively small, which easily achieves a low bending stiffness. With these special features, it is possible to apply these flexible acoustic wave devices to vibrate, to transmit, and receive modulated acoustic signals for variety of applications. However, this has not been widely explored.

In this paper, a multifunctional and flexible Lamb wave device operated based on the piezoelectric effect is applied for achieving integrated sensing, acoustic communication, and positioning functions. **Figure 1**a,b shows schematic illustrations and photographs of the proposed flexible Lamb wave devices. As the flexible Lamb wave devices are fabricated on thin substrates (with thicknesses generally less than 100 µm) with low stiffness, they can be forced to vibrate and transmit acoustic waves due to the piezoelectric effect when excited by low-frequency electrical signals (e.g., tens of kHz). Conversely, these flexible devices can also receive acoustic waves and generate net charges on the electrodes, which can be measured and converted into electrical signals, as shown in Figure 1c. The generated vibration mode, which is different from the Lamb waves traveling along the surface, results in the vibration of the whole membrane, thus transmitting and receiving acoustic energy. Therefore, such kind of acoustic wave is a promising candidate for wireless communications between flexible acoustic devices, especially when used underwater, as shown in Figure 1d. Based on this new methodology, the flexible Lamb wave sensor could be also served as an acoustic transceiver without any additional antennas, thus reducing the complications and size of the system. Furthermore, because of the low velocity of these acoustic waves, the acoustic ranging and positioning can be directly performed based on the time of flight or phase difference, as illustrated in Figure 1e,f, thus realizing significantly improved positioning precision than those based on Bluetooth and RFID (Radio Frequency Identification). Table S1 (Supporting Information) summarizes and compares

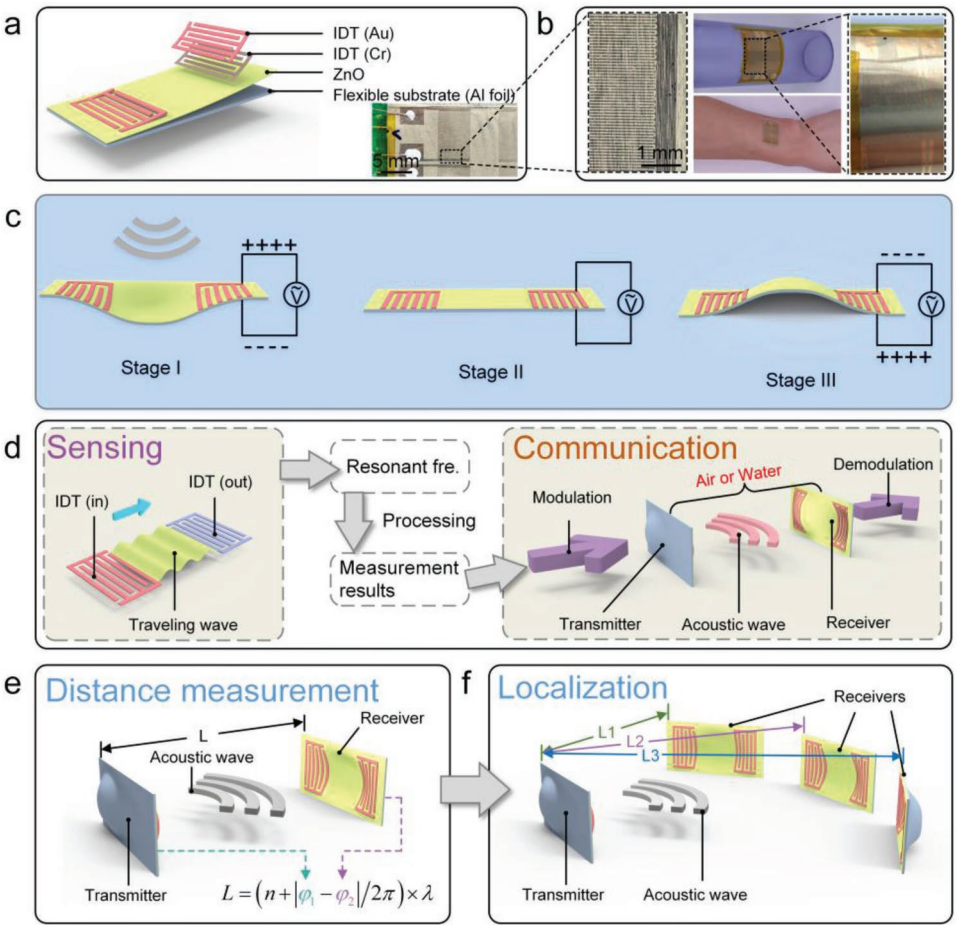

Figure 1. Architecture and working mechanism of the flexible acoustic wave device. Schematic illustrations of a) the structure of the flexible acoustic wave device, c) the transmitting and receiving of acoustic energy, the processes of d) sensing and communication, e) acoustic ranging, and f) positioning using the flexible acoustic wave devices. b) Photographs of the flexible acoustic wave device.

the key attributes of acoustic waves, bluetooth, and RFID for these applications.

For demonstration of this novel integrated multifunctional platform, the proposed flexible acoustic device is applied to realize the functions of sensing, communication, ranging, and positioning. This paper first investigates the influences of frequency and distance on the signal-to-noise ratio (SNR) of the received signal. Communication tests in both the air and underwater conditions are performed without using any additional antennas or communication modules. To verify the flexibility, communication tests are conducted using the flexible Lamb wave devices under different bending conditions (e.g., pasted on the surface of a pipe and on the upper arm of a volunteer). Taking respiratory monitoring as a demonstration, two flexible Lamb wave devices are used to perform real-time sensing and wireless communication, proving that the sensing and communication functions can be operated simultaneously without apparent interferences if properly configured. Furthermore, the performance of the proposed flexible Lamb wave device is evaluated for acoustic ranging and 2-dimensional (2D) positioning. An array of the proposed flexible devices can form WSNs with multiple functions, e.g., measuring the temperature field in a specific region (by sensing and positioning), real-time monitoring, and communication of a specific quantity (by sensing and communication). With the distinctive features of compactness, low power consumption, flexibility, and multifunctionality, the proposed smart WSN is scalable for applications in smart homes, wearable devices, medical health monitoring, and multi-robot coordination.

2. Experimental Section

2.1. Fabrication and Experimental Setup

Aluminum (Al) foils with a thickness of 50 μm were chosen as the flexible substrate to reconcile the flexibility with the acoustic performance of the device. The substrate could be served as a bottom electrode and confine the electric field. A zinc oxide film of ≈3.5 μm thick was deposited onto the Al foil as the piezoelectric layer due to its good film crystallinity, low film stress, and relatively good adhesion with various substrates.[34] Using DC (direct current) magnetron sputtering technology, a zinc target of 99.99% purity was sputtered at a power of 400 W, and the distance between substrate and target was ≈70 mm. A gas mixture of O_2 and Ar was introduced into the chamber at flow rates of 13 and 10 sccm, respectively, and the pressure of the chamber was maintained at ≈5 mTorr. On top of this ZnO piezoelectric layer was the upper electrode composed of interdigital transducers (IDTs), which were prepared using the conventional photolithography and lift-off processes. A single IDT was comprised of 35 pairs of Cr/Au (10 nm/80 nm thick) electrodes with a wavelength of 160 μm. Lamb waves were excited and received using the IDTs, which were characterized by the S21 parameters, and measured by a vector network analyzer (VNA, Agilent E5061B). The first four vibration modes (A0, S0, A1, and S1) were simulated using a simplified 2D model in COMSOL, and the obtained results are shown in Figure S1 (Supporting Information). These IDTs could also be cooperated with the bottom electrode to drive the piezoelectric material to emit ultrasound with a low frequency (tens of kHz).

To determine the optimal communication frequency, the maximum acoustic ranging distance, and the maximum transmission rate, various experiments were carried out using flexible acoustic devices. As shown in **Figure 2**a; Figure S5a (Supporting Information), two identical flexible acoustic devices, which were served as one transmitter and one receiver, were fixed on the printed circuit boards (PCBs) and placed facing each other with a distance varying from 0.2 to 4.2 m. The modulation signals were generated by a MATLAB program, and subsequently imported into an arbitrary waveform generator (Agilent 33522A). The transmitter was directly driven using the waveform generator with a peak voltage of 5 V and an output impedance of 50 Ω. The electrical signals produced by the receiver were first amplified using a charge amplifier (Femto HQA-15M-10T), subsequently measured by an oscilloscope (ZLG ZDS1104), and eventually imported into the computer for processing and demodulation. For demonstrating the principle using this prototype, it was quite convenient to use several instruments to perform these tests in the lab environment. For future applications with a specific product, the various functions including data processing and communication management could be realized using commercial integrated circuits, which are easily shrunk into miniaturized electronic devices.

2.2. Statistical Analysis

For presenting the communication results, the linear components were removed from the data by subtracting the best-fit straight line. For ease of observation, the signal envelopes are plotted after multiplying them by different factors ranging from 0.1 to 100, which are denoted as F in the figures. The normalized results, i.e., the demodulated signals, can be obtained using the following equation:

$$N = \frac{E - mean(E)}{\left|E - mean(E)\right|} \tag{1}$$

where N is the normalization result, E is the envelope of signal, and *mean* is a function of calculating the average value. To characterize the performance of distance measurement, the experiments were repeated three times, from which the mean values and standard deviations (SD) were derived. The data were presented with a format of mean value ± SD where the SD equals to half of the length of error bars. The calculations were performed using both MATLAB and Excel. All human experiments were performed with approval from the Zhejiang University Experimental Ethics Committee. Written consent was acquired from the volunteer of the research.

3. Results and Discussions

3.1. Wireless Communication via Acoustic Waves

Figure 2b schematically illustrates the acoustic communication system between the two flexible Lamb wave devices. For

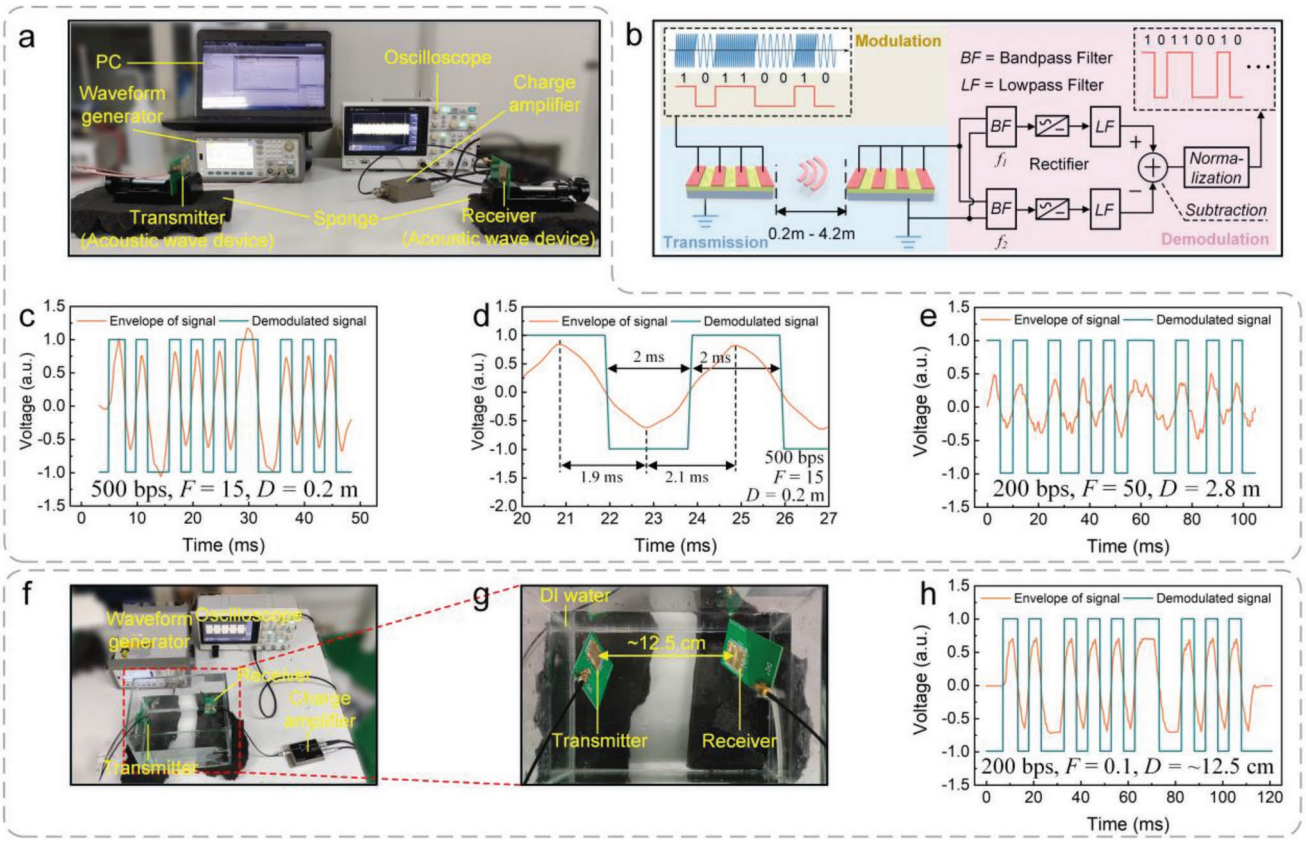

Figure 2. The communication performance using flat transmitters and receivers. a) The experimental setup for communication and signal processing using two flexible acoustic devices placed facing each other. b) Schematic illustration of the processes, including modulation, transmission, and demodulation. The demodulated signals obtained in communication experiments with distances of c) 0.2 m and e) 2.8 m. d) A close-up view of (c), demonstrating a response time of ≈2 ms. f) The experimental setup for underwater communication tests using two flexible acoustic devices placed facing each other, with a distance of ≈12.5 cm. g) A close-up view of (f). h) The demodulated signals obtained in the underwater experiments with a transmission rate of 200 bps. For ease of observation, the signal envelopes are plotted after multiplying them by factors denoted as F shown in the corresponding figures.

simplicity, binary frequency-shift keying (BFSK) is adopted as the modulation scheme.[12] The BFSK can be implemented using two carriers with different frequencies to modulate the digital signals of "0" and "1", respectively. The binary messages composed of "0" and "1" are modulated and fed into the transmitter. Hence, the transmitter is forced to generate modulated acoustic signals when stimulated with the corresponding electrical signals due to the inverse piezoelectric effect. The acoustic signals can be detected by the receiver and then transformed back into electrical signals due to the piezoelectric effect. The received signals are filtered using two band-pass filters corresponding to the carriers of "0" and "1" to obtain two-channel signals, which are rectified, and filtered using a low-pass filter to obtain their envelopes. The demodulated signal, i.e., the binary message, can be recovered by sequential dual-channel differentiation and normalization. The demodulation process was accomplished using a MATLAB program, which is presented in the Section of Demodulation in the Supporting Information.

To determine the optimal communication frequency, sine waves with frequencies from 2 to 2^{10} kHz were experimentally evaluated by stimulating the transmitter. The voltage amplitudes and SNRs of the received signals are shown in Figure S2a (Supporting Information). From the overall trends shown in this figure, both the voltage amplitudes and the SNRs are decreased with the increasing frequency. The SNR reaches a maximum value of 66.5 dB at a frequency of 16 kHz, hence 16 and 17 kHz are used for communication experiments because of their high SNRs. To investigate the maximum communication distance of the proposed flexible devices, a sine wave with a frequency of 16 kHz and an amplitude of 5 V was used to drive the transmitter. The transmitter and receiver were placed facing each other with a distance varied from 0.2 to 2.8 m. As shown in Figure S2b (Supporting Information), an increase of distance results in the reductions of both voltage amplitudes and SNRs of the received signals. With the distance increasing from 0.2 to 2.8 m, the voltage amplitude decreases from 395.5 to 1.5 mV and the SNR decreases from 70.9 to 22.0 dB. According to ref. [35], a threshold SNR of 12 dB was adopted for an ultrasonic rangefinder to avoid false recognition. With the same threshold SNR of 12 dB, the proposed flexible acoustic devices could achieve an effective distance of approximately several meters.

To evaluate the multibit communication performance of the proposed flexible acoustic device, a 21-bit binary stream (101001010101100101010) was modulated for transmission. Each

bit occupied a 2 ms duration in the transmission stage, corresponding to data rates of 500 bits per second (bps). With a distance of 0.2 m between the transmitter and the receiver, the received signals after demodulation are shown in Figure 2c, which indicates that the 21-bit binary message can be correctly transmitted and extracted depending on the proposed flexible acoustic devices. Figure 2d shows a close-up view of Figure 2c, including a bit of "1" and a bit of "0". Each bit occupies a duration of exactly 2 ms. However, the response times, which are ≈1.9and ≈2.1 ms, limit the maximum transmission rate. An excessively high transmission rate will lead to inter-symbol interference (ISI), which may result in bit errors. The response time is determined by the properties of the flexible device itself, but the multipath effect will also increase the response time, as schematically illustrated in Figure S3 (Supporting Information). In the indoor environment, the maximum communication rate decreases as the communication distance is increased due to the multipath effect. The distance between the transmitter and the receiver is further increased to 2.8 m, and the obtained results of the communication tests are shown in Figure 2e. Compared to the results in the case of 0.2 m distance, the voltage amplitudes of the received signals at 2.8 m distance are reduced, but the 21-bit binary message can be correctly transmitted nevertheless. Additionally, more severe ISIs are observed, possibly due to the more significant multipath effect in communication. As a result, the transmission rate is reduced to 200 bps to minimize bit errors. The received signals are displayed in time and frequency domains, as seen in Figure S4 (Supporting Information), demonstrating that the increase of distance from 0.2 to 2.8 m results in a reduction of SNR. For a communication distance of ≈4.2 m, the ISI makes it tough for the flexible device to maintain a transmission rate of 200 bps. To evaluate the communication performance, an 8-bit binary stream (11001010) was modulated and transmitted at 25 bps. As the experimental results shown in Figure S5 (Supporting Information), the message can be correctly transmitted and demodulated, demonstrating that the proposed acoustic communication scheme is applicable within an effective distance of ≈4.2 m at the cost of the transmission rate.

To investigate the underwater communication capability of the system, an experimental setup was designed and applied as shown in Figure 2f,g. Both the transmitter and receiver were completely immersed in deionized water at a distance of ≈12.5 cm. The acoustic communication system performs well at 200 bps, as shown in Figure 2h. Further experiments were conducted without the charge amplifier, as shown in Figure S6 (Supporting Information). The message could be correctly transmitted at a distance of ≈2 m and a transmission rate of 500 bps. The experimental results demonstrate the potential of the system to be operated underwater, broadening the application scenarios.

To investigate the applicability of the system inside a metal shell, we have further done the communication experiments with a transmitter inside an aluminum pipe and a receiver outside this pipe. As shown in Figure S7a (Supporting Information), the transmitter is pasted on the internal surface of the pipe, whose internal and external diameters are 11 and 10 cm, respectively. Both ends of the pipe are plugged with the sponge. The results of communication tests are shown in Figure S7b (Supporting Information). The data can be transferred correctly, demonstrating that the acoustic waves can be transferred from inside the aluminum pipe to the outside.

In brief, we have confirmed that the proposed flexible devices can serve as both transmitters and receivers for acoustic communication through the air in the indoor environment, with an effective distance of ≈2.8 m and a transmission rate of 200 bps. Operation at a larger distance (e.g., 4.2 m) will result in a lower maximum transmission rate because of the multipath effect. Furthermore, the flexible devices are applicable for communication through the water, which is desirable for these wearable devices in underwater usages.

3.2. Performance of Flexible Lamb Wave Sensor

The deformation of flexible devices is generally accompanied by variations of film's internal stress and mechanical properties, which may result in the degradation of the transceiver performance.[36] Therefore, the proposed acoustic communication scheme was further evaluated under several bending conditions.

As shown in **Figure 3**a, the flexible acoustic devices served as both the transmitter and receiver are pasted onto the external surface of a pipe with a diameter of 0.11 m, parallel to the pipe axis. The rest of the experimental setups are consistent with those explained in **Section 2**. For a transmission distance of 0.92 m, the demodulated waveform is shown in Figure 3b, from which the transmitted message can be accurately recovered.

Figure 3c shows a plot of changes in SNRs of the received signals versus the distance between the transmitter and receiver. The SNR decreases from 61.0 to 46.0 dB with the increase in the distance from 0.1 to 0.7 m, whereas the SNR increases from 46.0 to 48.5 dB with the increase in the distance from 0.7 to 0.92 m. This is because the transmission inside the pipe suffers from a more severe multipath effect than that in the outside ambient. By transmitting a single signal, multiple signals with the same frequency and different phases are captured and superimposed at the receiving end. The received signal is the superposition of all these signal vectors. Hence, the amplitude of the received signal does not necessarily decrease with the increase in communication distance. Furthermore, the SNRs obtained in the experiments on the pipe are ≈10 dB less than those in the experiments conducted in the air with flat transmitters and receivers, which might be attributed to the multipath effect and stress caused by bending.

To simulate the applications where the flexible acoustic devices are embedded into pipes or large equipment, the receiver is transferred to the internal surface of the pipe, as shown in Figure 3d. The distance between the transmitter and receiver is kept at 0.92 m. The received signals after demodulation are demonstrated in Figure 3e, which shows a relatively low SNR but is sufficient to extract the digital information.

Figure 3f shows the experimental setup for evaluating the performance of the flexible acoustic devices applied for wearable usages. The transmitter is attached to a flexible printed circuit board (FPC), and subsequently pasted on the volunteer's upper arm. The receiver is pasted on the external surface of the pipe. The distance between the transmitter and the receiver

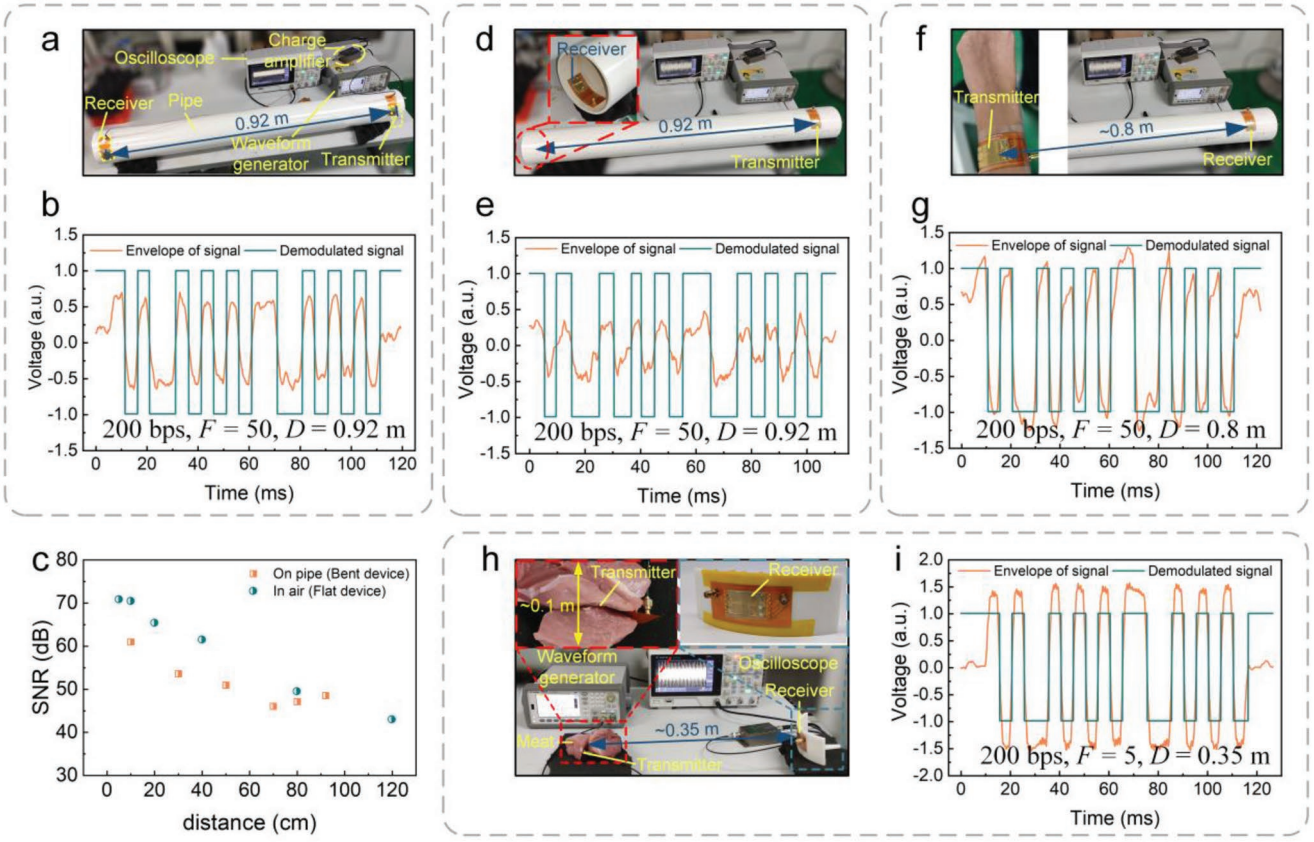

Figure 3. Photographs of experimental setups and the corresponding communication performances in various applications using bent transmitters and receivers. a,b) The transmitter and receiver are both pasted on the external surface of the pipe. c) The change in SNR of the received signal versus the distance between the transmitter and receiver. d,e) The transmitter and receiver are pasted on the external and internal surfaces of the pipe, respectively. f,g) The transmitter and receiver are pasted on the volunteer's upper arm and the pipe's external surface, respectively. h,i) The transmitter is sandwiched between two pieces of meat with thicknesses of ≈5 cm, and the receiver is fixed on the curved surface of a cylindrical shell. For ease of observation, the signal envelopes are plotted after multiplying them by factors denoted as F shown in the corresponding figures.

is ≈0.8 m. As demonstrated in Figure 3g, the binary message is accurately transmitted at 200 bps, indicating the reasonably good communication quality and broad prospects for integration for wearable applications of the proposed flexible devices.

Figure 3h shows that the transmitter of the acoustic device is sandwiched between two pieces of meat with a thickness of ≈5 cm each. The receiver is taped on the surface of a 3D-printed cylindrical shell, which is positioned at a distance of ≈35 cm from the transmitter. The results of the communication experiments obtained using this setup are shown in Figure 3i. Acoustic waves propagate through the meat to realize the transmission of signals, implying the prospect of the flexible device to be used for communication and sensing in biomedical applications, for example, used as the implantable medical devices.

In the above four demonstration cases, the time-domain and frequency-domain waveforms of the received signals are shown in Figure S8 (Supporting Information). Results show that the deformation could cause a shift in the optimal communication frequency. Therefore, when using such kind of flexible acoustic wave device, the communication frequencies should be calibrated prior to each experiment to optimize the performance.

The maximum transmission rates are principally determined by the response times, therefore, we further investigated these response times and compared those in the flat condition and the various bent conditions. As shown in Figure S9 (Supporting Information), the response times are almost unaffected by bending, which are ≈2.5 to 3 ms in all the cases, corresponding to the maximum transmission rate of 400 to 333 bps.

To investigate the communication performance of the device with different curvatures, the transmitter and the receiver were pasted on curved surfaces with various radii, including 5, 7.5, 10, −5, −7.5, and −10 cm, and placed face to face with a distance of 0.6 m. For each test, the two curved surfaces where the transmitter and receiver were pasted have the same radius. The experimentally obtained results are shown in Figure S10 (Supporting Information). The voltage amplitudes of the envelope of signals are affected by the changes of curvatures. In response to the bending, the resonant frequency of the flexible device is shifted, thus changing the amplitude of the responses. When the curved surface with a radius of −5 cm was used, the envelope of signal achieved the largest amplitude. Whereas when the surface with a radius of −10 cm was used, it shows the minimum amplitude. Nevertheless, all the binary messages were extracted correctly for all the six conditions, demonstrating the superior functionality of the proposed system.

The performance of the acoustic communication system was also investigated by repeated bending tests, where the transmitter and the receiver were bent (with a radius of ≈7.5 cm) and then flatten for 100 cycles. Figure S11a, b (Supporting Information) shows the initial performance of the acoustic communication system and its performance after bending for 100 cycles, respectively. The messages are transmitted correctly for both cases at 200 bps with a distance of 0.6 m. Figure S11c (Supporting Information) shows comparisons of the signals obtained before and after the bending cycles, and the voltage amplitude only decreases slightly after bending cycles.

In summary, the proposed flexible acoustic transmitters and receivers perform well in various flexible and bending conditions, e.g., pipes with severe multipath effects, wearable, and implantable applications. Before their usage, the flexible devices are required to be calibrated by sweeping the frequency in a small range to determine the optimal communication frequencies.

3.3. Real-Time Respiratory Monitoring and Communication

Monitoring of respiration, one of the vital signs for human beings, is becoming increasingly important, especially for patient monitoring in clinical environments,[37] diagnosis of respiratory disorders (e.g., sleep apnea,[2] asthma,[38] Cheyne-Stokes, or Biot's respiration),[39] and wearable technology for sport applications.[39] For these applications, one special advantage of using our proposed flexible acoustic device is its versatility in multiple functions, including sensing, transmitting, and receiving.

To demonstrate the feasibility of cooperative operations involving multiple functions in real-time and non-invasive respiratory monitoring, we designed an experimental setup as shown in **Figure 4**a. As the exhaled breath reaches the surface of the flexible Lamb wave device, hot and humid airflow will raise the temperature of the device. If the humidity is over-saturated, the water molecules are condensed on the surface of the device. As a result, the resonant frequency of the Lamb wave device will be changed passively in response to the breath. By measuring the resonant frequency shifts, respiration can be monitored in real-time. To implement the sensing and communication system, one flexible acoustic device is served as both sensor and transmitter, and another one is served as a receiver, as shown in Figure 4a. The S21 transmission parameters of the two-port Lamb wave sensor are measured using the VNA, and recorded by the LabVIEW and MATLAB program, which reads the values of the resonant frequencies and sends them to the microcontroller through the serial port. The microcontroller modulates the digital signals and directly drives the transmitter with a voltage amplitude of 5 V to yield the corresponding acoustic signals, which are converted back into electrical waveforms by the receiver. These signals are then

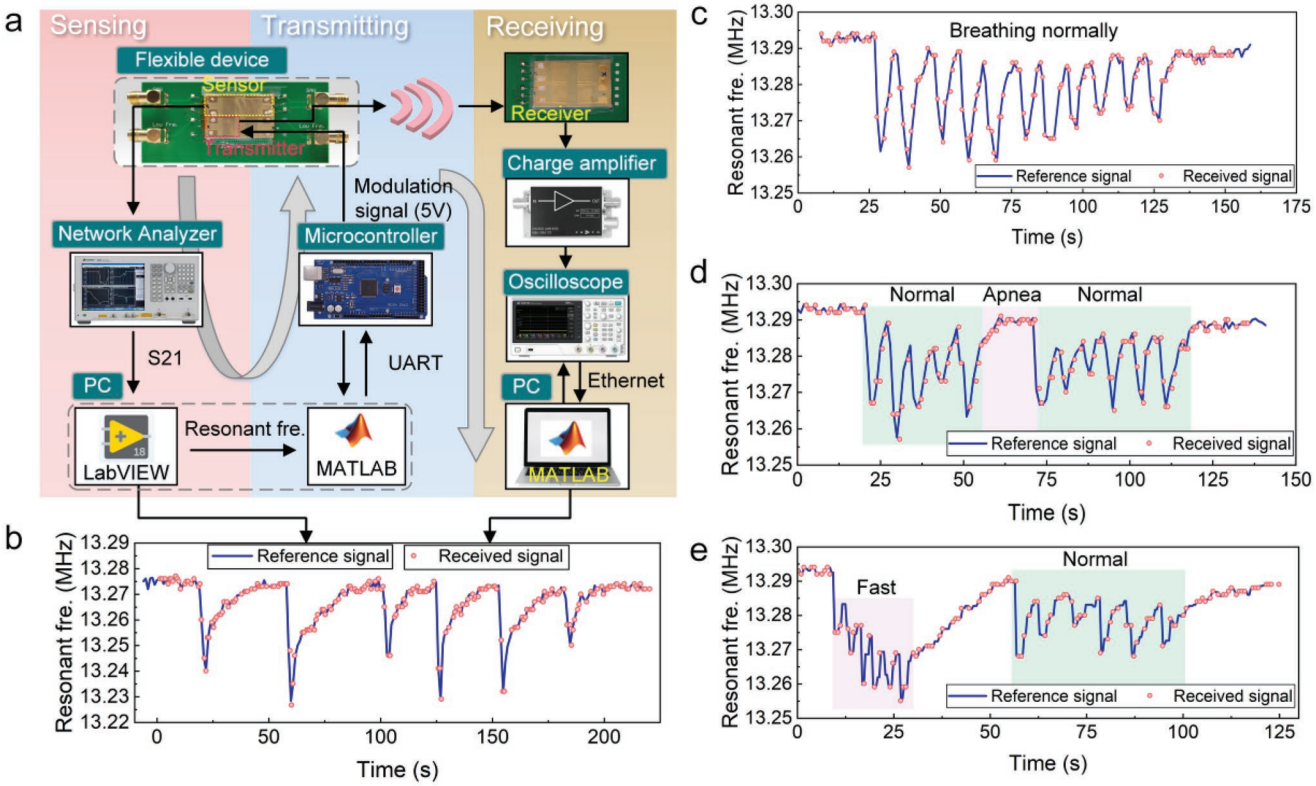

Figure 4. Real-time breath monitoring and wireless information transmission. a) The experimental setup for real-time respiratory monitoring and wireless transmission of the measurement results. b) The resonant frequencies changing passively in response to respiration, shown as a function of time. The reference signal indicates the resonant frequencies measured directly by the VNA. The received signal indicates the resonant frequencies extracted from the waveforms measured by the receiver. c) The frequency responses to normal breathing. d) The frequency responses during the breath and apnea processes. e) The frequency responses to fast and normal breathing.

amplified by a charge amplifier and can be read out using an oscilloscope. Another MATLAB program at the receiving end is responsible for communicating with the oscilloscope, reading the waveform, extracting the digital information, and also displaying it in real-time. During the measurements, the Lamb waves were always generated. The acoustic waves for communication were generated periodically (with a period of ≈0.8 s), lasting for 0.4 s, to transmit the measurement results. The circuit diagram is shown in Figure S12 (Supporting Information), which illustrates the detailed electrical connections used in these experiments.

Figure 4b shows the variations of the recorded resonant frequencies of the Lamb wave sensor induced by the breathing of a volunteer. A decrease in its resonant frequency upon exhalation is observed, and after exhalation, the resonant frequency increases over time until the start of the next exhalation. The "reference signals" represent the resonant frequencies measured directly by the VNA. The "received signals" are the recorded resonant frequencies, which are transmitted in binary form, and extracted from the received waveforms. Obviously, the "reference signals" can be accurately reproduced from the "received signals" as shown in Figure 4b, which demonstrates that the sensing and communication functions of the acoustic wave device are operated simultaneously without apparent interference. Although the acoustic communication in this study cannot reach the transmission rate as high as in those of RF connections in air, it is still adequate for the application which needs to transmit the results measured by the flexible device in real-time.

To demonstrate the applicability of the system for various breathing patterns, several experiments were further conducted. Figure 4c,d show the frequency responses during the normal breathing and sleeping apnea cases, respectively. The resonant frequency shows an obviously different pattern for the paused breath. Figure 4e shows the obtained resonant frequencies when the flexible device was exposed to fast (0.3 Hz) and normal (0.14 Hz) breathing, indicating the applicability of the monitoring system in both two conditions. However, the resonant frequency shows a gradually downward shift while measuring the fast respiration, which is not clearly observed in the normal breathing results. This is mainly because the response time is short enough for the flexible device to recover to the initial state in the measurement of normal breathing, but this is not the case for the fast-breathing measurement.

Coated with different sensitive materials, these Lamb wave devices have previously been reported for numerous sensing applications (e.g., temperature,[40] humidity,[41] UV,[23] strain,[42] and biochemical substances).[20] Therefore, the proposed flexible device and corresponding acoustic communication system, with their multiple functions, could have broad application prospects in wireless scenarios, including but not limited to respiratory monitoring.

3.4. Acoustic Ranging and Positioning

Positioning is a fundamental requirement in the cooperative operation of multiple sensors, and it is also an important function in forming a multi-sensor network. To implement the positioning function, the acoustic ranging between two flexible acoustic devices was investigated, i.e., one for transmitting and the other for receiving. Since the speed of sound in air at 25 °C is only 346 m s^{-1}, the distance can be measured by phase differences and expressed using the following equation [43]

$$L = \left(n + \Delta\varphi/2\pi\right) \times \lambda, n = 0,1,2... \tag{2}$$

where L is the distance between the transmitter and the receiver, $\Delta\varphi$ is the phase difference between the transmitting and receiving signals, λ is the wavelength of the acoustic wave, and n is an integer not less than 0. However, the value of n cannot be easily determined unless the maximum range is less than the λ. In order to expand the maximum range, the method based on multi-frequency continuous wave is adopted.[44] In this study, three different frequencies are used for acoustic ranging, denoted as f_1, f_2, and f_3, and their corresponding phase differences are marked as p_1, p_2, and p_3. The estimation of the distance takes the form of the equation (3) [43]

$$\begin{aligned} L = {} & \mathrm{Int}\left(\frac{|p_1 - p_2|}{2\pi} \times \frac{|f_1 - f_3|}{|f_1 - f_2|}\right) \times \frac{c}{|f_1 - f_3|} \\ & + \mathrm{Int}\left(\frac{|p_1 - p_3|}{2\pi} \times \frac{f_1}{|f_1 - f_3|}\right) \times \frac{c}{f_1} + \frac{|p_1 - p_2|}{2\pi} \times \frac{c}{f_1} \end{aligned} \tag{3}$$

where L is the distance between the transmitter and the receiver, c is the sound velocity in air, and Int() is the integer operation. The maximum range and minimum resolution are determined by the choice of the frequencies. The maximum range can be calculated using the equation (4) [43]

$$L_{\max} = c/\min\left(\left|f_i - f_j\right|\right), i, j = 1,2,3 \tag{4}$$

The minimum resolution is given by equation (5)[43]

$$R_{\min} = c/\left[\max\left(\left|f_i - f_j\right|\right) \times 2\pi\right], i, j = 1,2,3 \tag{5}$$

where min() and max() indicate the operations to find the minimum and maximum values, respectively. To evaluate the acoustic ranging performance, a maximum range of ≈1 m was determined in consideration of the trade-off between range and resolution. The following studies selected three frequencies of 18, 18.7, and 19 kHz for their better performance. The obtained maximum range and minimum resolutions are 115 cm and 5.51 cm rad^{-1}, respectively.

The experimental setup for the positioning tests is shown in **Figure 5**a. The signals, including the three frequency components, are synchronously produced at the two ports of the waveform generator. One signal is fed into the oscilloscope as a reference, and the other one is fed into the transmitter with an amplitude of 5 V to generate the corresponding acoustic signals. The receiver placed facing the transmitter converts the received acoustic signals back into electrical ones, which are subsequently amplified by the charge amplifier and recorded using the oscilloscope.

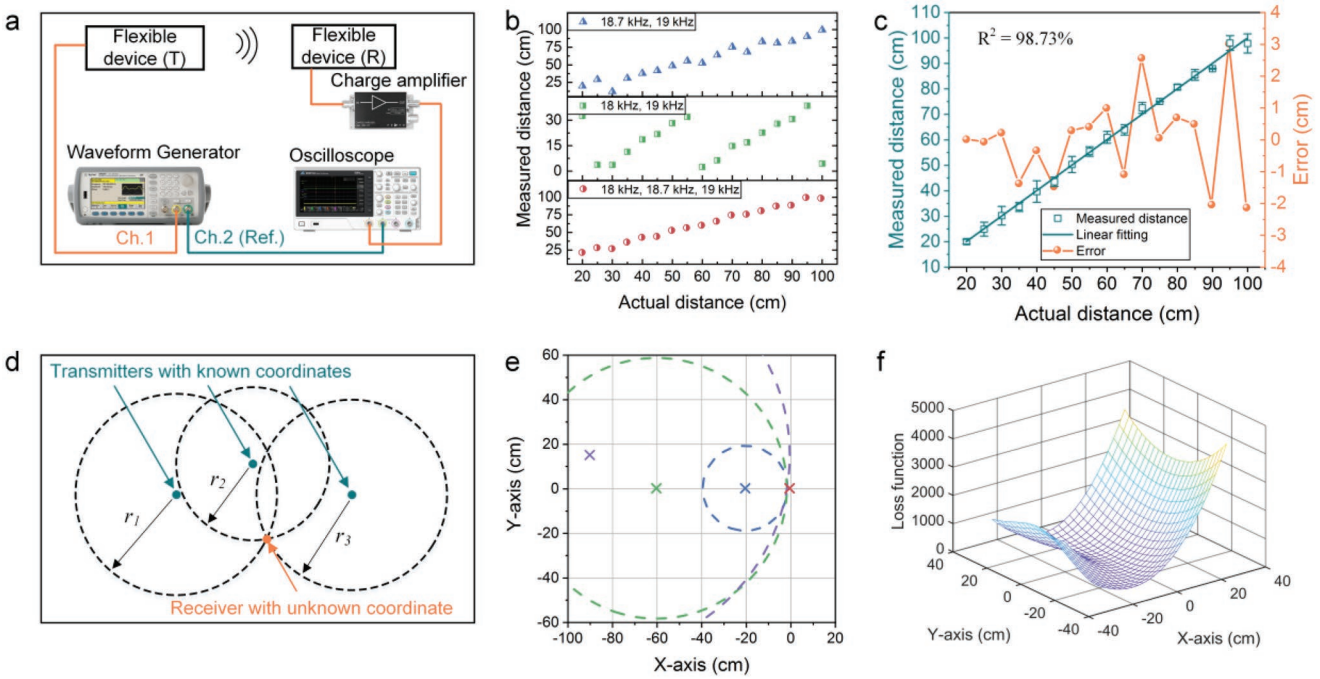

Figure 5. Ranging and positioning via the flexible acoustic devices. a) The experimental setup for ranging between two flexible acoustic wave devices. b) The measured distance presented as a function of the actual distance from 20 to 100 cm, calculated by 18.7/19, 18/19, 18/18.7/19 kHz phase shift difference, respectively. c) The fitted linear plot and error plot of the ranging results calculated by 18/18.7/19 kHz phase shift difference. d) Schematic diagram of positioning principle. The unknown coordinate of the receiver can be estimated by the intersection of the three circles. e) The experimental results of positioning shown by the three circles and their corresponding centers in colors of blue, green ,and purple, respectively. f) The loss function displayed as a function of coordinates of estimation. Error bars in panel (c) indicate the standard deviation ($n = 3$).

The obtained results of acoustic ranging, which were measured by increasing the distances between the transmitter and the receiver from 20 to 100 cm, are shown in Figure 5b. The distance measurement using two different frequencies could be expressed by equation (6)

$$L = \frac{p_1 - p_2}{2\pi} \times \frac{c}{f_1 - f_2} \tag{6}$$

where f_1 and f_2 are the frequencies used for the measurement, p_1 and p_2 are the phase shifts corresponding to the f_1 and f_2, and c is the sound velocity. The measurement results based on frequency signals of 18.7 and 19 kHz show a large measured acoustic range but also a large error. On the contrary, the measurement results based on frequency signals of 18 and 19 kHz show a relatively small acoustic range but a small error. The nonlinear behavior is mainly due to that the measuring distance exceeds the maximum range, thus the phase difference between the actual value and the calculated result is $2n\pi$ (n = 1, 2, 3...). Analyzing all the measured data for three cases of 18, 18.7, and 19 kHz, both large range and small error can be obtained, demonstrating that the ranging performance can be improved by increasing the number of frequencies. The distance measurements from 20 to 100 cm were conducted independently for three times, and the averaged results of the estimated distances were obtained, as shown in Figure 5c. The maximum error is less than 3 cm for a measurement range of 100 cm. A linear regression is further performed on the averaged results with a slope constrained to be 1, and the regression results exhibit good linearity with an R^2 of 98.73%.

The mechanism of 2D localization is schematically illustrated in Figure 5d. The three transmitters with known coordinates were arranged in a non-collinear geometry. The distances between the receiver with unknown coordinates and all the transmitters were measured, respectively. Three circles were determined with the coordinates of the three transmitters as centers and the corresponding three distances as radii. These three circles should theoretically intersect at a point, i.e., the coordinate of the receiver. Nevertheless, due to the measurement errors, the three circles generally did not have a common intersection in the experiments. To address this issue and determine the optimal estimation of the receiver's coordinate, a loss function is chosen and defined as

$$Loss(x,y) = \sum_{i=1}^{3}\left(\sqrt{(x - x_{ti})^2 + (y - y_{ti})^2} - r_i\right)^2 \tag{7}$$

where (x_{ti}, y_{ti}) are the coordinates of the three transmitters, (x, y) is the coordinates of the receiver, and r_i are the three distances measured between the transmitters and the receiver. The optimal estimation of the receiver's coordinate was then obtained by minimizing the loss function, and the obtained experimental results of positioning are shown in Figure 5e. The coordinates of these three transmitters, which are represented by the blue, green, and purple symbols of "×", are

Table 1. Details of the positioning experiment.

	Transmitters (Known)			Receiver (Actual)	Receiver (Estimated)
Coordinates [cm]	(–20, 0)	(–60, 0)	(–90, 15)	(0, 0)	(–1.1, 0.7)
r [cm]	19.13	58.75	90.08		

(–20, 0 cm), (–60, 0 cm), and (–90, 15 cm), respectively. The actual coordinate of the receiver is (0, 0 cm), which is represented by the red "×". As shown in Figure 5f, the loss function has a minimum value of 0.0751 at (–1.1, 0.7 cm), which is consequently taken as the measured coordinate of the receiver, corresponding to a measurement error of ≈1.3 cm. The detailed positioning results are summarized in **Table 1**. The measured distances from the receiver to the three transmitters are 19.13, 58.75, and 90.08 cm, respectively. In conjunction with the known coordinates of the transmitters, the estimation of the receiver's coordinates can be calculated as (–1.1, 0.7 cm), as indicated by Figure 5f.

To sum up, the proposed acoustic system demonstrates an excellent capacity for 2D positioning of a flexible acoustic device with unknown coordinates based on the phase difference of acoustic signals, which is constructive for handling the localization problems of large-scale WSNs.[45] The flexible and multifunctional acoustic system with such a special positioning function is promising for future applications, e.g., gait recognition,[46–48] indoor positioning systems,[49,50] and parking guidance.[51]

4. Conclusion

In this paper, we report a multi-functional flexible sensor network based on thin-film acoustic wave devices, offering a novel insight to extend the functionality of a single device to cooperative operations of multiple units. Transmission and reception of low-frequency acoustic waves (≈20 kHz) in air and water are achieved based on the piezoelectric effect, and short-range communication and ranging/positioning have been demonstrated accordingly.

Acoustic communications have further been experimentally conducted using two of such flexible acoustic devices, one of which is served as the transmitter and another as the receiver, at a transmission rate of 200 bps within a range of ≈2.8 m and at a transmission rate of 25 bps within a range of ≈4.2 m. Communications in underwater conditions are performed without using a charge amplifier at a transmission rate of 500 bps within a range of ≈2 m. Under various bent conditions (for wearable and implantable applications), the proposed acoustic communication system consistently exhibits a good transceiver performance. As a demonstration of multi-device collaboration, the real-time respiratory monitoring and continuous transmission of the measurement results have been performed using two flexible devices, proving that the sensing and communication functions can be operated simultaneously under proper scheduling.

Using the method of multi-frequency continuous waves, we have demonstrated acoustic ranging within 1 m using the proposed flexible devices, with a maximum error of 3 cm and $R^2 = 98.73\%$. For further validation of positioning, the distances from the receiver were measured separately by three transmitters with different coordinates, based on which the unknown coordinate of the receiver has been estimated with an error of ≈1.3 cm. We believe the proposed flexible wireless sensor system is a promising candidate for next-generation WSNs, providing a novel wearable health and activity monitoring strategy, indoor positioning system, and industrial predictive maintenance.

Supporting Information

Supporting Information is available from the Wiley Online Library or from the author.

Acknowledgements

This work was supported by the "National Natural Science Foundation of China (52175552, 52075162, 51875521)" and the "Zhejiang Provincial Natural Science Foundation of China (LZ19E050002)", the Innovation Leading Program of New and High-tech Industry of Hunan Province (2020GK2015, 2021GK4014), the Joint Fund Project of the Ministry of Education, the Excellent Youth Fund of Hunan Province (2021JJ20018), the UK Engineering and Physical Sciences Research Council (EPSRC) under grant EP/P018998/1, and International Exchange Grant (IEC/NSFC/201078) through Royal Society UK and the NSFC.

Conflict of Interest

The authors declare no conflict of interest.

Data Availability Statement

The data that support the findings of this study are available from the corresponding author upon reasonable request.

Keywords

acoustic communication, acoustic waves, flexible devices, indoor positioning, respiratory monitoring, smart wireless sensors, wearable sensors

Received: August 20, 2022
Revised: October 11, 2022
Published online: November 27, 2022

[1] C. Y. Sik, J. Hyoyoung, R. T. Yin, A. Raudel, P. Anna, Y. Jaeyoung, L. J. Yoon, T. Andreas, L. Y. Joong, S. W. Chen, H. S. Knight, K. Seungyeob, A. Hak-Young, W. Grace, V.-G. Abraham, H.-D. Elizabeth, B. A. Russo, M. A. Napolitano, T. J. Holleran, R. L. Abdul, A. N. Miniovich, L. Geumbee, G. Beth, K. Brandon, H. Shuling, J. A. Brennan, A. Kedar, K. S. Soo, K. Joohee, W. E. Alexandria, et al., *Science* **2022**, *376*, 1006.
[2] N. Zavanelli, H. Kim, J. Kim, R. Herbert, M. Mahmood, Y. S. Kim, S. Kwon, N. B. Bolus, F. B. Torstrick, C. S. D. Lee, W. H. Yeo, *Sci. Adv.* **2021**, *7*, abl4146.

[3] E. McGlynn, V. Nabaei, E. Ren, G. Galeote-Checa, R. Das, G. Curia, H. Heidari, *Adv. Sci.* **2021**, *8*, 2002693.
[4] S. Niu, N. Matsuhisa, L. Beker, J. Li, S. Wang, J. Wang, Y. Jiang, X. Yan, Y. Yun, W. Burnett, A. S. Y. Poon, J. B. H. Tok, X. Chen, Z. Bao, *Nat. Electron.* **2019**, *2*, 361.
[5] H. Seungyong, K. Jeonghyun, W. S. Min, M. Yinji, K. Daeshik, X. Zhaoqian, L. Kyu-Tae, C. H. Uk, B. Anthony, M. Seunghwan, H. S. Yun, C. R. Davies, L. J. Woo, L. Chi-Hwan, K. B. Hoon, L. Kan, Z. Yadong, W. Chen, F. Xue, H. Yonggang, J. A. Rogers, *Sci. Transl. Med.* **2018**, *10*, aan4950.
[6] R. Lin, H.-J. Kim, S. Achavananthadith, S. A. Kurt, S. C. C. Tan, H. Yao, B. C. K. Tee, J. K. W. Lee, J. S. Ho, *Nat. Commun.* **2020**, *11*, 444.
[7] X. Tian, P. M. Lee, Y. J. Tan, T. L. Y. Wu, H. Yao, M. Zhang, Z. Li, K. A. Ng, B. C. K. Tee, J. S. Ho, *Nat. Electron.* **2019**, *2*, 243.
[8] Y. Haitao, Y. B. Seng, L. Zhipeng, L. Kerui, C. Ting-Hsiang, J. Lin, L. Yang, J. S. Ho, R. Hongliang, C. Po-Yen, *Sci. Robot.* **2019**, *4*, aax7020.
[9] Y. Shao, L. Wei, X. Wu, C. Jiang, Y. Yao, B. Peng, H. Chen, J. Huangfu, Y. Ying, C. J. Zhang, J. Ping, *Nat. Commun.* **2022**, *13*, 3223.
[10] Y. Park, K. Kwon, S. S. Kwak, D. S. Yang, J. W. Kwak, H. Luan, T. S. Chung, K. S. Chun, J. U. Kim, H. Jang, H. Ryu, H. Jeong, S. M. Won, Y. J. Kang, M. Zhang, D. Pontes, B. R. Kampmeier, S. H. Seo, J. Zhao, I. Jung, Y. Huang, S. Xu, J. A. Rogers, *Sci. Adv.* **2022**, *6*, abe1655.
[11] W. Lu, W. Bai, H. Zhang, C. Xu, A. M. Chiarelli, A. Vázquez-Guardado, Z. Xie, H. Shen, K. Nandoliya, H. Zhao, K. Lee, Y. Wu, D. Franklin, R. Avila, S. Xu, A. Rwei, M. Han, K. Kwon, Y. Deng, X. Yu, E. B. Thorp, X. Feng, Y. Huang, J. Forbess, Z.-D. Ge, J. A. Rogers, *Sci. Adv.* **2022**, *7*, abe0579.
[12] C. Li, D. A. Hutchins, R. J. Green, *IEEE Trans. Ultrason. Ferroelectr. Freq. Control* **2008**, *55*, 908.
[13] X. Huang, J. Saniie, S. Bakhtiari, A. Heifetz, In *2020 IEEE Int. Conf. Electro Info. Technol. (EIT)*, IEEE, Piscataway, NJ **2020**, pp. 206–210.
[14] T. F. Bechteler, H. Yenigun, *IEEE Trans. Microw. Theory Tech.* **2003**, *51*, 1584.
[15] K. Chawla, G. Robins, L. Zhang, In *IEEE 5th Int. Symp. Wireless Pervasive Comput.* IEEE, Piscataway, NJ **2010**, pp. 301–306.
[16] M. Bouet, G. Pujolle, *Comput. Commun.* **2009**, *32*, 1485.
[17] L. Zhang, C. Gao, Y. Jiang, B. Liu, M. Zhang, H. Zhang, Q. Li, X. Chen, W. Pang, *Adv. Electron. Mater.* **2019**, *5*, 1800545.
[18] H. Jin, J. Zhou, X. He, W. Wang, H. Guo, S. Dong, D. Wang, Y. Xu, J. Geng, J. K. Luo, W. I. Milne, *Sci. Rep.* **2013**, *3*, 2140.
[19] L. Lamanna, F. Rizzi, F. Guido, L. Algieri, S. Marras, V. M. Mastronardi, A. Qualtieri, M. De Vittorio, *Adv. Electron. Mater.* **2019**, *5*, 1900095.
[20] L. Lamanna, F. Rizzi, V. R. Bhethanabotla, M. De Vittorio, *Biosens. Bioelectron.* **2020**, *163*, 112164.
[21] L. Lamanna, F. Rizzi, V. R. Bhethanabotla, M. De Vittorio, *Sens. Actuators A* **2020**, *315*, 112268.
[22] J. Wu, C. Yin, J. Zhou, H. Li, Y. Liu, Y. Shen, S. Garner, Y. Fu, H. Duan, *ACS Appl. Mater. Interfaces* **2020**, *12*, 39817.
[23] X. L. He, J. Zhou, W. B. Wang, W. P. Xuan, X. Yang, H. Jin, J. K. Luo, *J. Micromech. Microeng.* **2014**, *24*, 055014.
[24] R. Tao, J. Reboud, H. Torun, G. McHale, L. E. Dodd, Q. Wu, K. Tao, X. Yang, J. T. Luo, S. Todryk, Y. Fu, *Lab Chip* **2020**, *20*, 1002.
[25] J. Chen, H. Guo, X. He, W. Wang, W. Xuan, H. Jin, S. Dong, X. Wang, Y. Xu, S. Lin, S. Garner, J. Luo, *J. Micromech. Microeng.* **2015**, *25*, 115005.
[26] H. Xu, Z. Cao, S. Dong, J. Chen, W. Xuan, W. Cheng, S. Huang, L. Shi, S. Liu, U. Farooq, A. Qadir, J. Luo, *J. Micromech. Microeng.* **2019**, *29*, 025003.
[27] J. Zhou, Z. Ji, Y. Guo, Y. Liu, F. Zhuo, Y. Zheng, Y. Gu, Y. Fu, H. Duan, *npj Flex. Electron.* **2022**, *6*, 84.
[28] Z. Ji, J. Zhou, H. Lin, J. Wu, D. Zhang, S. Garner, A. Gu, S. Dong, Y. Fu, H. Duan, *Microsyst. Nanoeng.* **2021**, *7*, 97.
[29] L. Piro, L. Lamanna, F. Guido, A. Balena, M. Mariello, F. Rizzi, M. De Vittorio, *Nanomaterials* **2021**, *11*, 1479.
[30] R. Tao, G. Mchale, J. Reboud, J. M. Cooper, H. Torun, J. T. Luo, J. Luo, X. Yang, J. Zhou, P. Canyelles-Pericas, Q. Wu, Y. Fu, *Nano Lett.* **2020**, *20*, 3263.
[31] J. Zhou, X. He, H. Jin, W. Wang, B. Feng, S. Dong, D. Wang, G. Zou, J. K. Luo, *J. Appl. Phys.* **2013**, *114*, 044502.
[32] X. Yang, J. Liang, Y. Jiang, X. Chen, H. Zhang, M. Zhang, W. Pang, *IEEE Electron Device Lett.* **2017**, *38*, 1125.
[33] Y. Jiang, Y. Zhao, L. Zhang, B. Liu, Q. Li, M. Zhang, W. Pang, *Small* **2018**, *14*, 1703644.
[34] Y. Q. Fu, J. K. Luo, N. T. Nguyen, A. J. Walton, A. J. Flewitt, X. T. Zu, Y. Li, G. McHale, A. Matthews, E. Iborra, H. Du, W. I. Milne, *Prog. Mater. Sci.* **2017**, *89*, 31.
[35] Z. Zhou, S. Yoshida, S. Tanaka, *Sens. Actuators A* **2017**, *266*, 352.
[36] Q. Zhang, Y. Wang, D. Li, X. Yang, J. Xie, Y. Fu, *Appl. Phys. Lett.* **2021**, *118*, 121601.
[37] K. van Loon, B. van Zaane, E. J. Bosch, C. J. Kalkman, L. M. Peelen, *PLoS One* **2015**, *10*, 0144626.
[38] C. Massaroni, C. Venanzi, A. P. Silvatti, D. L.o Presti, P. Saccomandi, D. Formica, F. Giurazza, M. A. Caponero, E. Schena, *J. Biophotonics* **2018**, *11*, 201700263.
[39] T. Hoffmann, B. Eilebrecht, S. Leonhardt, *IEEE Sens. J.* **2011**, *11*, 1112.
[40] R. Tao, S. A. Hasan, H. Z. Wang, J. Zhou, J. T. Luo, G. McHale, D. Gibson, P. Canyelles-Pericas, M. D. Cooke, D. Wood, Y. Liu, Q. Wu, W. P. Ng, T. Franke, Y. Q. Fu, *Sci. Rep.* **2018**, *8*, 9052.
[41] X. Tao, H. Jin, M. Mintken, N. Wolff, Y. Wang, R. Tao, Y. Li, H. Torun, J. Xie, J. Luo, J. Zhou, Q. Wu, S. Dong, J. Luo, L. Kienle, R. Adelung, Y. K. Mishra, Y. Q. Fu, *ACS Appl. Nano Mater.* **2020**, *3*, 1468.
[42] H. Xu, S. Dong, W. Xuan, U. Farooq, S. Huang, M. Li, T. Wu, H. Jin, X. Wang, J. Luo, *Appl. Phys. Lett.* **2018**, *112*, 093502.
[43] C. F. Huang, M. S. Young, Y. C. Li, *Rev. Sci. Instrum.* **1999**, *70*, 1452.
[44] X. Chen, J. Xu, H. Chen, H. Ding, J. Xie, *J. Microelectromech. Syst.* **2019**, *28*, 634.
[45] Y. Shang, W. Rumi, Y. Zhang, M. Fromherz, *IEEE Trans. Parallel Distrib. Syst.* **2004**, *15*, 961.
[46] Y. Qi, C. B. Soh, E. Gunawan, K.-S. Low, R. Thomas, *IEEE Trans. Neural Syst. Rehabil. Eng.* **2016**, *24*, 88.
[47] S. Liu, J. Zhang, Y. Zhang, R. Zhu, *Nat. Commun.* **2020**, *11*, 5615.
[48] Y. Qi, C. B. Soh, E. Gunawan, K. Low, *IEEE J. Biomed. Health Inform.* **2015**, *19*, 446.
[49] C. Medina, J. C. Segura, Á. De la Torre, *Sensors* **2013**, *13*, 3501.
[50] M. Hazas, A. Hopper, *IEEE Trans. Mob. Comput.* **2006**, *5*, 536.
[51] M. Chen, T. Chang, In *2011 IEEE Int. Conf. Inf. Autom.*, IEEE, Piscataway, NJ **2011**, pp. 601–605.